RSC Advances

This is an *Accepted Manuscript*, which has been through the Royal Society of Chemistry peer review process and has been accepted for publication.

Accepted Manuscripts are published online shortly after acceptance, before technical editing, formatting and proof reading. Using this free service, authors can make their results available to the community, in citable form, before we publish the edited article. This *Accepted Manuscript* will be replaced by the edited, formatted and paginated article as soon as this is available.

You can find more information about *Accepted Manuscripts* in the Information for Authors.

Please note that technical editing may introduce minor changes to the text and/or graphics, which may alter content. The journal's standard Terms & Conditions and the Ethical guidelines still apply. In no event shall the Royal Society of Chemistry be held responsible for any errors or omissions in this *Accepted Manuscript* or any consequences arising from the use of any information it contains.

ROYAL SOCIETY OF CHEMISTRY

www.rsc.org/advances

Please do not adjust margins

RSC Advances

ARTICLE

A Reference Material of Single-walled Carbon Nanotubes: quantitative chirality assessment using optical absorption spectroscopy

Received 00th January 20xx,
Accepted 00th January 20xx

DOI: 10.1039/x0xx00000x

www.rsc.org/

Ying Tian [a,b,†,*], Hua Jiang [b,†], Ilya V. Anoshkin [b], Lauri. J.I. Kauppinen[b], Kimmo Mustonen[b], Albert G. Nasibulin [b,c,d], Esko I. Kauppinen [b]

A reference material is essential to enable and accelerate commercialization of new materials. The National Institute of Standards and Technology (NIST) of the United States recently released the world's first reference material of a single-walled carbon nanotube (SWCNT) dispersion known as RM8281. Although the description of the material have been well documented by NIST, the chirality population, one of the most important properties, is yet unidentified for the RM8281. Here, we present for the first time a quantitative chirality assessment of the RM8281 reference material by using a method based on optical absorption spectroscopy. A universal background model has been established for SWCNT solid film samples, which proves to be the key to the successful chirality assessment. Our results show that approximately 75 % of SWCNTs in RM8281 have diameters distributing in a narrow range of 0.7 - 0.9 nm, and about 69 % of SWCNTs have chiral angles ranging from 15° to 30°. For the whole population, semi-conducting SWCNTs (~74 %) prevail significantly over metallic ones (~26%). Importantly, ~ 25 % of the total RM8281 SWCNT population was found to be *(6,5)* nanotube. High-resolution transmission electron microscopy and electron diffraction technique were utilized to complete an adequate statistical analysis of chirality distribution in RM8281, giving a satisfactory agreement with the above absorption spectrum measurements, thus, validating absorption spectroscopy serving as a fast and standard protocol for quantifying the SWCNT chirality population.

Introduction

In 2013, The National Institute of Standards and Technology (NIST) in the United States released the world's first reference material RM8281 for dispersed single-walled carbon nanotube (SWCNT). RM8281 is comprised of a set of length-sorted SWCNT dispersions specified as long, medium and short fractions[1]. As a reference sample for measurement comparison and applications, it is vital to build up a complete database containing all important structure parameters. The accompanying user information of RM8281 documented by NIST has provided with comprehensive structure information characterized using multiple techniques, including transmission electron microscopy (TEM), atomic force microscopy (AFM), UV-Vis-NIR optical absorbance spectroscopy (OAS), Raman spectroscopy and fluorescence spectroscopy (FS). The homogeneity of the RM8281 was assessed both by using the absorbance ratio at certain wavelength in OAS, as well as the G/D and G'/G peak ratio in Raman spectra[2]. As a reference sample, RM8281 has been successfully applied to develop a universal protocol to evaluate the purity of bulk SWCNT samples[3]. This protocol ensures the reproducibility of such evaluation, thus allows inter-laboratory comparisons and metrology development without concerns of sample variation.

The properties of a SWCNT depend largely on its chiral structure, termed "chiralities", identified by two integers *n* and *m* describing the "roll-up" vector of a graphene lattice to form the SWCNT. Thus, the chirality distribution of a SWCNT sample plays key roles in directing its commercial applications. NIST usually provides with a UV-Vis-NIR absorbance spectrum (AS) for each population of RM8281 in the Report of Investigation when RM8281 are delivered to customers. By looking into the peak features of those spectra, one can qualitatively identify a few chiral species including semiconducting *(6,5)*, *(7,5)*, *(7,6)*, *(8,3)*, *(8,4)*, and *(9,1)* species and metallic *(6,6)*, *(7,4)*. However, no complete data set for the *(n,m)* population in RM8281 have yet been available.

One attempt has been made to analyze the *(n,m)* populations by combining AS and FS [4-6]. With better resolved peak positions of semiconducting SWCNTs (S-SWCNTs) identified in FS as constraints, the AS can be fitted to reveal

[a] *Department of Physics, Dalian Maritime University, Dalian, Liaoning 116026, China.*
[b] *Department of Applied Physics, Aalto University School of Science, Puumiehenkuja 2, Espoo, 00076, Finland.*
[c] *Skolkovo Institute of Science and Technology 100 Novaya st., Skolkovo, Moscow, 143025, Russia*
[d] *Laboratory of Hybrid Materials for Electronics and Optoelectronics, Peter the Great Saint-Petersburg Polytechnic University, Polytechnicheskaya 29, Saint Petersburg, 195251, Russia*
† Y.Tian and H.Jiang contributed equally to this work.

RSC Advances Accepted Manuscript

Please do not adjust margins

even the small shoulder peaks, thus to achieve a more reliable *(n,m)* distribution. However, such methods work only with SWCNTs in dispersions that fluoresce, and generally provide a relatively accurate assessment of S-SWCNT abundance, but a poor evaluation for metallic-SWCNT (M-SWCNT) assignment. Other calculations for *(n,m)* abundance using AS usually involve an independent integration of the three main peak areas, which correspond to the first (E_{11}^S) and second transition energy (E_{22}^S) of S-SWCNT, and the first transition energy (E_{11}^M) of M-SWCNT, respectively [7-10]. *A priori* separation of the absorption spectrum into three regions and the subsequent independent simulation ignore the possibility of peak overlapping arising from different electronic transitions. Moreover, all of the above methods used empirical backgrounds that were subtracted at the peak minima to approximate the absorption from electronic transitions of SWCNT and underlying background absorption from the π-plasmon[11-14]. Such empirical background subtractions usually cause a significant deviation on the determination of the absorption peak position and area, thus lead to a deviated analysis of SWCNT chirality type and population. It is worth to remarking that the absorption background of SWCNTs in dispersion varies significantly with a number of external factors, including the selection of the surfactant, preparation procedures and chemical doping, etc[15]. With these factors affecting the absorption background, it is particularly challenging to establish a standard protocol for reproducible quantitative analysis of absorption spectra based on the SWCNT dispersion samples.

In this work, we have developed an enhanced AS analytical technique to complete an assessment of chirality population in the long fraction RM8281 sample. In order to avoid the afore-mentioned problems in AS analysis for dispersion samples, a dry solid film of the RM8281 sample was used in our work. The absorbance background resulting physically from the M-point exciton transition and π plasmon was successfully identified for the RM8281 solid film. This background can be utilized as a universal model to accurately subtract the background for the SWCNT solid film samples. After the background being subtracted, the entire absorption profile is modelled to be linear composition of the absorbance from each (n,m) SWCNT in the sample, thus, it is unnecessary to manually force the spectrum being divided into three regions. With this routine, a full structure characterization of the RM8281 sample including S-SWCNT/M-SWCNT ratio, diameter, chiral angle and chirality distributions has been achieved. Finally, high-resolution TEM (HRTEM) and electron diffraction (ED) analytical techniques were utilized to validate the above AS results by directly measuring nearly three hundred individual and bundled SWCNTs for statistical analysis of chirality distribution in the same sample. The high degree of agreement between TEM results and those from our AS analysis with the enhanced technique demonstrates that AS technique is a simple and efficient protocol for quantitative evaluation of chirality distribution in SWCNT samples. More importantly, our results have provided the RM8281 users with a full data set of chirality population in this reference sample, thus will significantly promote its wide applications in various field.

Results and discussion

Figure 1 (a) shows the photograph of the RM8281 sample provided by NIST[16]. The long fraction RM8281 with an average nanotube length of 0.3 μm was studied in this work. A drop of RM8281 dispersion was cast onto a holey carbon film-*coated* copper mesh TEM grid. Then it was washed with several solvents, and annealed at 300 °C in high vacuum to remove the surfactant. As seen from the overview TEM image in Figure 1 (b), plenty of individual as well as SWCNT bundles are presented in the sample. Although some residual surfactant was observed at the edge of SWCNT bundles, very clean and well-crystallized individual and small bundles are obtained as shown in the HRTEM images (insets of Figure 1 (b)). It is noted that the small nanoparticles displayed in the image are copper particles originated from the copper grid during the annealing treatment (Fig. S1 in supporting information).

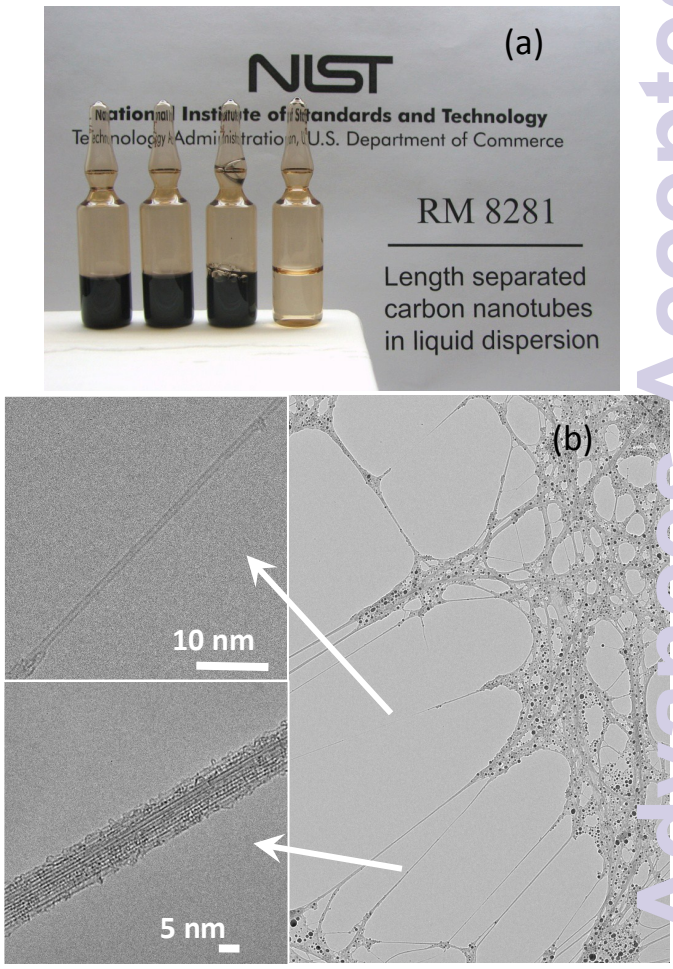

Fig. 1 (a) Photograph of the NIST RM8281 (left to right) the Long, Medium, and Short length-sorted nanotube dispersions (left to right) and a blank solvent. Reproduced with permission.[16] Copyright 2012, Nano Res. (b) TEM images of the RM8281 SWCNT sample. The

RSC Advances Accepted Manuscript

This journal is © The Royal Society of Chemistry 20xx

insets of (b) present the high-resolution TEM images of individual (top) and bundle (bottom) SWCNTs, respectively.

Figure 2 presents the absorption spectra of the RM8281 measured from dispersion (dotted line) and from solid thin film (solid line) samples, respectively. It can be seen that a broad and nearly featureless background is shown underneath the optical transition peaks in the near infrared (NIR) and visible (VIS) ranges and culminates at the ultraviolet (UV) region. Nevertheless, the high broad background at UV region can hardly be distinguished in the AS of the dispersion sample due to the strong absorbance from the employed solvent. Furthermore, recent studies show that the absorption baselines vary largely for different SWCNT dispersions due to a number of extrinsic factors, such as surfactant, sonication and centrifuge processing, *etc*[15,17]. This makes it difficult to identify the background and to further establish a universal protocol for the AS analysis on the basis of dispersion samples.

On the contrary, as shown in Figure 2 (solid line), the AS of the SWCNT solid film presents clear and full features at the UV region and can totally avoid the strong influences induced by the extrinsic factors in the dispersion sample. The high absorption peaks in the energy range of 4-6 eV further extend as a broad absorption baseline in the visible and NIR region. The UV absorption features at ~ 5.3 and ~ 4.5 eV have been generally assigned to be perpendicular and parallel components of π plasmons, respectively[18,19]. However, the experimental study[20] of the dielectric environment effects on the ~ 5.3 and ~ 4.5 eV components exhibited remarkable different behaviors, i.e., significant spectra change and no spectra change, respectively. This phenomenon conflicts with the conventional π -plasmon assignment for the 4.5 eV absorption feature, since all carbon atoms of SWCNTs are on the surface, therefore, π electrons should be affected by the surrounding environment, thus, raising a fundamental question as to its physical origin.

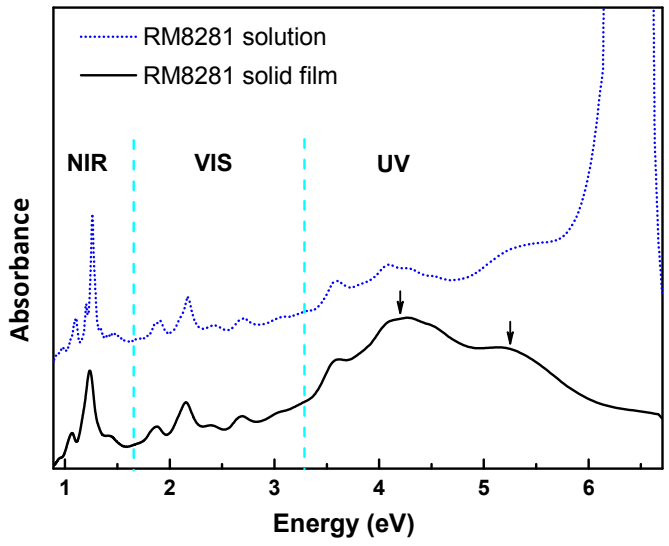

Fig. 2 The absorption spectra of RM8281 SWCNTs in solution (dotted line) and in solid thin film (solid line) along with clear absorption peaks in UV region (denoted by arrows). The Near infared (NIR), visible (VIS) and Ultraviolet (UV) regions are also indicated in the spectrum.

In the case of graphite, the origin of the strong UV absorption peak at 4.5 eV is well known and recognized as $\pi \rightarrow \pi^*$ interban electronic transition at the M saddle point of the Brillouin zone[21] This feature was also observed in graphene[22-24] as well as SWCNT aggregates recently[25]. Meanwhile, the experimental studies[19-21] presented that the strong electron-hole (e-h) interactions near a saddle-point singularity should be considered to explain the asymmetry profile of this 4.5 eV peak and the large redshift of the interband transition energy (compared with the values predicted within a single-particle picture). Such e-h interactions give rise to the unstable excitonic states lying below the saddle-point singularity in graphene and SWCNT aggregates systems, and consequently coupling with the existing continuum states with a high rate. This process leads to the asymmetric resonance feature that can be well described by the asymmetry Fano line shape absorption[24,25] Therefore, we fit the UV absorption in two components: the lower energy component (~ 4.5 eV) having a Fano lineshape that corresponds to the M-point exciton transition, and the higher one (~ 5.3 eV) having a lorentzian lineshape that corresponds to π plasmon resonance. For a Fano profile $A(E) \propto (q+\varepsilon)^2/(1+\varepsilon^2)$ where $\varepsilon = (E - E_{res})/(\Gamma/2)$. Here E_{res} is the exciton resonance energy, Γ corresponds to broadening of the peak width, and q^2 defines the ratio of the strength of the excitonic transition to free $\pi \rightarrow \pi^*$ transition. The parameters of peak widths and positions of the two components in the UV region are variable in the least-squares fitting, and are finally obtained when the best fitting of the UV absorption features is achieved. The best fit to this model yields $E_{res} = 4.32\ eV$, $\Gamma = 638$ meV (≈ 6 fs) and $q = -3.47$. As shown in the Figure 3 (a), the Fano and Lorentzian line shapes fit the UV absorption peaks very well. In particular, the Fano tail fits extremely well the broad absorption background underneath the resonant transition peaks in the visible and NIR region. And this background model established in the SWCNT aggregates can be extended as a standard protocol for the background subtraction of SWCNT solid film samples.

After the background subtraction, the absorbance is modelled as a linear composition of each nanotube type[17] and each optical transition is assumed to be Lorentzian profile which was generally used to describe the interband transitions [26], as shown below

$$A_{SWNT}(E) = \sum_{(n,m)} \omega_{(n,m)}\, A_{(n,m)}(E) \qquad (1)$$

$$A_{(n,m)}(E) = \sum_{ii} \frac{1}{\pi \Delta E\left[1+\left(\frac{E-E_{ii}^{(n,m)}}{\Delta E}\right)^2\right]} \qquad (2)$$

Here, $\omega_{(n,m)}$ returns the fraction of the (n,m) SWCNT in the bulk. The (n,m) chirality concentration in a SWCNT sample can be obtained by $C_{(n,m)} = \omega_{(n,m)} / \sum_{(n,m)} \omega_{(n,m)}$. Thus the fitting parameters in this model are peak position (i.e., transition energy $E_{ii}^{(n,m)}$ (i=1,2,3...)), peak width (ΔE), as well as absorption cross section of each SWCNT, which will be described as follows. The values of transition energy were taken from the recent experimental work on the optical transitions of SWCNTs [27]. The broadening factor ΔE from 50 to 110 meV was tested in fitting process, and it appears that the value of 80 meV fits the best for the fitting of RM8281 SWCNT solid thin film sample. This is in agreement with the value of

RSC Advances Accepted Manuscript

ΔE obtained from the AS of single chirality SWCNT[28]. The absorption cross sections are assumed to be the same for all nanotube. The absorption cross section has been proven to be chirality-dependent [29, 30], but currently there is still a lack of a full experimental dataset of absorption cross section covering all chiralities. However, recent experimental results indicate that the absorption cross section of a SWCNT depends largely on its diameter [31]. Since the RM8281 has a narrow diameter range of 0.7-0.9 nm, it is acceptable to assume an equal absorption cross section, independent of (n,m), for the fitting. All SWCNTs with diameters in the range of 0.5-1.5 nm are considered in the fitting process without imposing any weight factors for certain chiralities prior to the fitting. This direct linear problem of finding the coefficients of $\omega_{(n,m)}$ is ill-conditioned. This problem can be solved[17] by the canonical regularization, i.e., $min_{\omega}\|A(\omega) - A_{measured}\|_2^2 + c\|\omega\|_2^2$, and with the regularization parameter c=3 giving reasonable results.

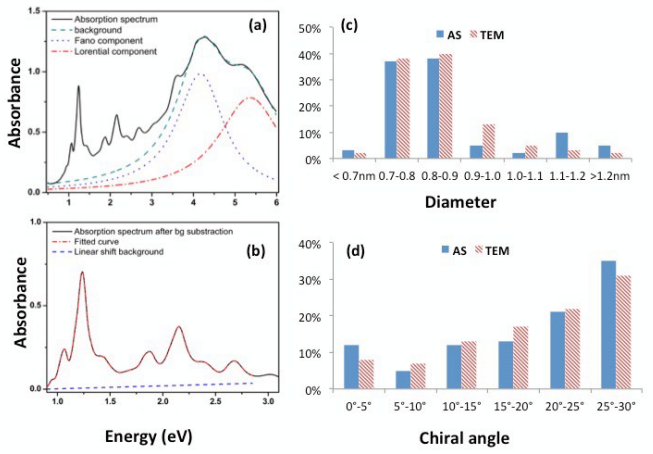

Fig. 3 (a) The absorption spectra of RM8281 SWCNT thin film along with Fano (dotted blue line) and Lorential backgrounds (dashed and dotted red line) which correspond to the Saddle-point exciton transition and π plasma, respectively. (b) The absorption spectrum after background subtraction (black solid line) and the corresponding calculated absorption spectrum (dashed and dotted red line) along with a linear shift background (blue dashed line). (c) The diameter and (d) chiral angle distributions of RM8281 SWCNTs obtained from absorption spectra (in solid bins) and TEM, ED (in textured bins), respectively.

Figure 3 (b) shows the background-free absorption spectrum of the RM8281 thin film (solid line) and the corresponding fitted spectrum (dash dot line) achieved by the least-square fitting procedure. The difference between the experimental and fitted spectra can hardly be seen with a minor deviation of 1.4 %. Since a linear shift background has been employed to compensate the uncertainty of the background assumption in our previous work [17], the tiny linear shift background indicated as dashed line in the Figure 3 (b) implies the accuracy of the background model.

Figure 3 (c) and (d) show histograms of the diameter and chiral angle distributions in the RM8281 SWCNTs achieved based on the AS simulation (solid bins). The deduced diameter histogram from AS shows that 75% SWCNTs in the RM8281 sample are located in the narrow diameter range of 0.7-0.9 nm. The chiral angle distribution of the RM8281 SWCNTs is biased towards the armchair direction and yields 69% SWCNTs with chiral angle from 15° to 30°. Meanwhile, a chirality map of the RM8281 sample is obtained as shown in Figure 4. The results show that the *(6,5)* tube represents the major chirality with a concentration of 25% in the RM8281 sample, far more than those *(6,6)*, *(7,5)* and *(8,3)* with each being close to 10%, respectively. The chiralities having around 5% of content in the sample include *(8,4)*, *(8,5)*, *(9,3)*, *(10,7)*, *(10,8)*, *(11,0)*, *(11,5)*. Meanwhile, the obtained S-SWCNT fraction of the RM8281 is about 74%.

It has been widely utilized to obtain the S-SWCNTs populations from the E_{11}^S *and* E_{22}^S spectral features in AS [7,11]. Thus, we also tried to calculate the chiratliy distribution of S-SWCNTs by only fitting the E_{11}^S *and* E_{22}^S spectral features. The fitting results of both chirality types and concentrations are consistent with the chirality histogram of S-SWCNTs obtained by fitting the whole spectrum (Fig. S2 in supporting information). This further testifies the validity and advantages of our strategy of not splitting the absorption spectrum into different regions prior to fitting.

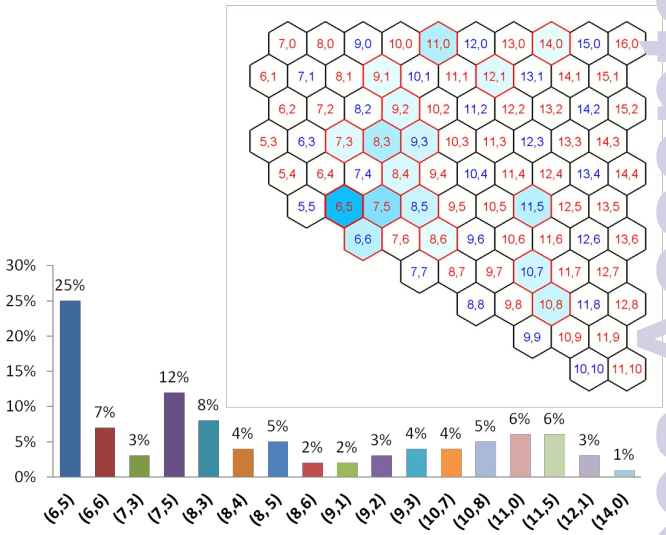

Fig. 4 Chirality (n,m) map of RM8281 SWCNTs obtained based on absorption spectrum.

The assessment of chirality population in RM8281 sample by using the above spectroscopy measurements have been further validated by utilizing the HRTEM and ED, which allow direct observation and quantitative characterization of the nanotube structure. For this purpose, a total of nearly three hundred SWCNTs i.e., including 89 isolated individual and 212 bundled SWCNTs were measured for statistical analysis of diameter, chiral angle and chirality distributions. It is known that conventional TEM images can hardly measure accurately the diameter of a SWCNT since the image contrast of a SWCNT depends strongly on focusing conditions as well as the spherical aberration coefficient of the microscope. In this work, the aberration-corrected HRTEM imaging technique is used for accurate measurement of carbon nanotube diameters [32], thus have led to dramatically

RSC Advances Accepted Manuscript

This journal is © The Royal Society of Chemistry 20xx

increased resolution, sensitivity and signal to noise, allowing imaging SWCNTs with high precision. In practice, the microscope is uniquely calibrated at a certain imaging condition with a SWCNT of known chirality (diameter) identified using ED technique. After that, all investigated SWCNTs are imaged at the same condition, maintaining consistency of measuring tube diameters from their high-resolution images. With this protocol, the error for the diameter measurements is estimated to be less than 1 %. We have measured 288 SWCNTs, giving a statistically sound nanotube diameter distribution as shown by the histogram (textured bins) in the Figure 3 (c). The results present the narrow distribution with 78% SWCNTs fall into the scale of 0.7-0.9 nm, which agrees very well with that obtained from AS measurement.

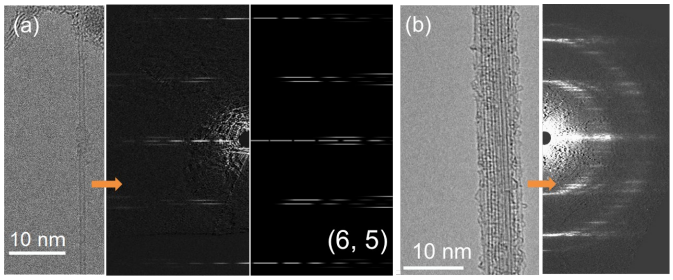

Fig. 5 (a) HRTEM image of an individual SWCNT and its ED patterns (left: Experimental ED, right: simulated image). (b) HRTEM image of a SWCNT bundle and the corresponding ED pattern.

From the SWCNTs of RM8281 as observed in Figure 1, high quality ED patterns can be obtained for the chirality and chiral angle analysis from both the individual (Figure 5 (a)) and small bundles (Figure 5 (b)) of SWCNTs. From the ED patterns of individual SWCNTs, chiral indices *(n,m)* can be determined unambiguously by using a unique method of intrinsic layer line distance analysis that was introduced by Jiang *et al* [33]. The axial distances of layer lines measured from the central equatorial line are scaled by the pseudo-periodicity of the equatorial oscillation to give dimensionless intrinsic layer line distances that can directly lead to calculations of the chiral indices n and m. The determination is completely free of the calibration of the diffraction pattern. With this method, the diffraction pattern shown in Figure 5 (a) has been indexed and the chiral indices of the SWCNT were determined to be *(6,5)* with the tube diameter of 0.75 nm and the chiral angle of 27°. A simulated ED pattern of the *(6,5)* nanotube is given in Figure 5 (a) (right) that shows good agreement with the experimental ED pattern showing in Figure 5 (a) (left).

When SWCNTs form bundles (Figure 5 (b) left), the above-mentioned method does not apply to determine their chiral indices. However, from the electron diffraction pattern of a SWCNT bundle, e.g. shown in Figure 5 (b) (right), a critical dimension characteristic of the C-C atomic bond length can be discerned, with the aid of which every single diffraction layer line from the SWCNT bundle can be easily identified and paired with its conjugated layer line, resulting in a single helicity contained in the bundle. If the density of layer lines is high and clustered into bunches, helicity bounds can be well defined, thus the chiral angle distribution ranges are calculated [34]. The error for the chiral angle evaluation from electron diffraction analysis is estimated to be less than 0.2 deg. In this work, a total of 301 data points have been obtained by electron diffraction analysis of both individual and bundle SWCNTs, which results in a chiral angle distribution histogram shown in Figure 3 (d) in textured bins. The results yield 70% SWCNTs with chiral angle from 15 to 30 °, which is in extremely good agreements with the fitting results from AS measurement, which gives 69% SWCNTs in the chiral angle range of 15-30 °. Thus, the independent multiple techniques present excellent agreements on the diameter and chiral angle properties of the same RM8281 sample.

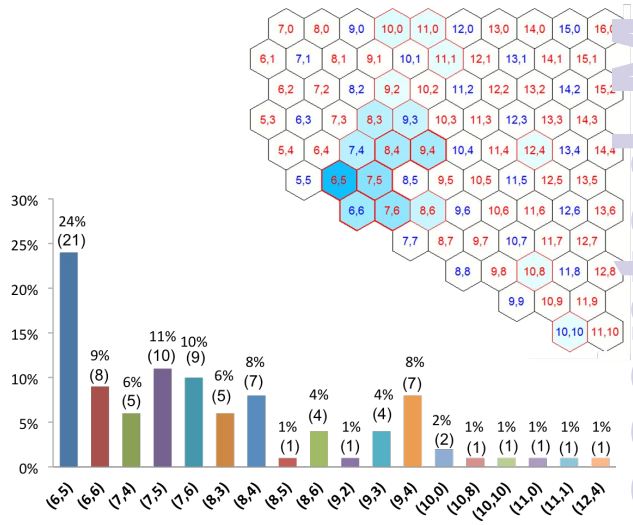

Fig. 6 Chirality (n,m) map of RM8281 SWCNTs based on ED analysis from a total of 89 isolated individual SWCNTs. Both concentrations and tube numbers (in bracket) of (n,m) SWCNTs are presented in the figure.

Figure 6 presents a chirality map of the RM8281 that was achieved by using the aforementioned calibration-free ED analysis on 89 isolated individual SWCNTs. In general, the sample takes on a relatively wide range of chirality distribution with a total of 17 observed chiralities. The *(6,5)* tube represents the major chirality that accounts for 24% in the RM8281 SWCNT sample. This result is consistent with the chirality histograms deduced from AS investigation (Figure 4) in which the major *(6,5)* concentration is 25%. Populations of other main chiralities such as *(6,6), (7,5), (8,3), (8,4), (8,5), (8,6), (9,2), (9,3)* that were achieved by ED analysis are also analogous to those obtained by AS. The main difference is that the chiralities of *(7,6)* and *(7,4)* presented in the ED measurements are missing in the AS calculation, while the AS simulates more metallic chiralities such as *(10,7), (10,8)* and *(11,5)*. The reasons for that are the overlapping absorbance features and the close transition energies of different chirality SWCNTs. For example, the E_{11}^S and E_{22}^S of the *(7,6)* SWCNT are 1.12 and 1.93 eV, respectively. The E_{11}^S of *(7,6)* is very close to the E_{11}^S of *(9,2), (12,1)* and *(11,0)* which are 1.11, 1.08 and 1.20 eV, respectively. And the E_{22}^S (1.93 eV) of *(7,6)* is micro-close to the E_{22}

RSC Advances Accepted Manuscript

(1.94 eV) of *(7,5)* SWCNT. The fitting program lacks power to resolve transition energies which are too close to each other, thus yields higher concentrations for *(7,5), (9,2), (11,0)* and *(12,1)* SWCNTs. In addition, the assumption of equal absorption cross section independent of (n,m) can also lead to the deviation of fitting results. The obtained S-SWCNT concentration from ED measurement is about 79%, which is consistent with the results of 74% obtained from the AS fitting. In general, we have shown that the AS technique can efficiently complete a quantitative assessment of structure distribution of the RM8281 SWCNTs, including diameter, chiral angle, chirality distributions and S-/M-SWCNT fraction, which gives a satisfactory agreement with the results obtained from TEM and ED measurements.

Conclusions

In summary, the chirality population of the NIST RM8281 SWCNT reference sample was investigated by using an enhanced method for absorption spectrum analysis. The obtained results show that the main chirality of RM8281 is *(6,5)* with a concentration of 25%. Other chiralities such as *(6,6), (7,5), (8,3), (8,4), (8,5), (8,6), (9,2), (9,3)* are also present in the RM8281 with concentrations varying from 3% to 12%. The tube diameters of the RM8281 distribute mainly between 0.7-0.9 nm and the chiral angles cluster favourably from 15 to 30°. The population of S-SWCNT (74%) overwhelms the M-SWCNT (26%) fraction. HRTEM and ED techniques were employed to validate the AS analysis. An adequate statistical analysis on nearly three hundred individual and bundle RM8281 SWCNTs, present a solid statistic of structure distributions: diameter, chiral angle, chirality and S-/M-SWCNT ratio. An excellent agreement between spectroscopic and microscopic techniques suggests that the extended AS analysis approach could be employed as a standard protocol for determining the chirality population of a SWCNT sample. Importantly, the census of the chirality population in the RM8181 sample fill in the gap of the missing structure information in the world´s first reference material of SWCNT, thus, will largely push forward its wide applications.

Experimental

The SWCNT sample studied in this report was synthesized by a CoMoCAT method and distributed by NIST[16] as a NIST reference material for dispersed, length sorted, carbon nanotubes (RM8281 'long' fraction). This sample contains approximately 2.5 ml of a length-sorted SWCNT dispersion in aqueous 1% (mass/vol) sodium deoxycholate solution. The estimated concentration of the nanotubes in the solution sample is 50 mg/L and the average length is approximately 0.3 µm. A solid film of RM8281 was obtained by vacuum filtering the SWCNT dispersion through an aluminium oxide membrane filter (Whatman Anopore with 0.2 µm pore size) with a smooth and flat surface. The remaining surfactant was rinsed sequentially with ethanol, iso-propanol, deionised water and acetone (~50 ml of each solvent for several times until bubbles disappeared in the filtrate). Then the membrane of SWCNT layer was placed in 0.05 M KOH solution. After 7 days, the SWCNT layer was detached from the etched filter surface, then was transferred onto a quartz substrate. The alkaline residue was washed out by 0.1 M HCl solution and deionized water until reaching the neutral pH value, then dried in vacuum to form the thin film sample.

High resolution TEM imaging and electron diffraction measurements were carried out by using a JEOL-2200FS double aberration-corrected microscope, operated at 80 kV that is well below the electron knock-on damage threshold for carbon [15,35]. Absorption spectra are acquired using a double beam Perkin-Elmer Lambda 950 UV-Vis-NIR spectrometer that covers the working wavelength range from 175 to 3300 nm. An uncoated substrate was used in the reference beam to exclude the effect of the substrate.

Acknowledgements

We are grateful to J. A. Fagan (NIST) for providing the RM8281 sample used in this work under the support of VAMAS project. We thank M. Zheng (NIST) and I. Bondarev (North Carolina Central University) for the fruitful discussions related to the analysis of AS. This work was funded by Academy of Finland, TEKES project CARLA, the European Union's Seventh Framework Program (IRENA project), Aalto Energy Efficiency program through the MOPPI project, National Natural Science Foundation of China (51502031), Fundamental Research Funds for the Central Universities of China (3132015139) and Liaoning Educational Committee Foundation (L2014208). A.G.N thanks the supporting from Ministry of Education and Sciences of the Russian Federation through project RFMEFI58114X0006. This work made use of the Aalto University Nanomicroscopy Center (Aalto-NMC) premises.

Notes and references

1. Reference Material RM 8281, https://www-s.nist.gov/srmors/view_detail.cfm?srm=8281.
2. Report of Investigation RM 8281, https://www-s.nist.gov/srmors/view_report.cfm?srm=8281.
3. V. M. Irurzun, M. P. Ruiz and D. E. Resasco, *Carbon*, 2010, **48**, 2873-2881.
4. G. Lolli, L. Zhang, L. Balzano, N. Sakulchaicharoen, Y. Tan and D. E. Resasco, *The Journal of Physical Chemistry B*, 2006, **110**, 2108-2115.
5. Y. Yuan, L. Wei, W. Jiang, K. Goh, R. Jiang, R. Lau and Y. Chen, *Journal of Materials Chemistry A*, 2015, **3**, 3310-3319.
6. Y. Xu, E. Dervishi, A. R. Biris and A. S. Biris, *Materials Letters*, 2011, **65**, 1878-1881.
7. N. Nair, M. L. Usrey, W.-J. Kim, R. D. Braatz and M. S. Strano, *Analytical Chemistry*, 2006, **78**, 7689-7696.
8. A. Hagen and T. Hertel, *Nano Letters*, 2003, **3**, 383-388.
9. R. Bhowmick, B. M. Clemens and B. A. Cruden, *Carbon*, 2008, **46**, 907-922.

RSC Advances Accepted Manuscript

 This journal is © The Royal Society of Chemistry 20xx

10. S. Ohmori, T. Saito, M. Tange, B. Shukla, T. Okazaki, M. Yumura and S. Iijima, *The Journal of Physical Chemistry C*, 2010, **114**, 10077-10081.
11. M. E. Itkis, D. E. Perea, S. Niyogi, S. M. Rickard, M. A. Hamon, H. Hu, B. Zhao and R. C. Haddon, *Nano Letters*, 2003, **3**, 309-314.
12. T. Pichler, M. Knupfer, M. S. Golden, J. Fink, A. Rinzler and R. E. Smalley, *Physical Review Letters*, 1998, **80**, 4729-4732.
13. X. Liu, T. Pichler, M. Knupfer, M. S. Golden, J. Fink, H. Kataura and Y. Achiba, *Physical Review B*, 2002, **66**, 045411.
14. D. Selbmann, B. Bendjemil, A. Leonhardt, T. Pichler, C. Täschner and M. Ritschel, *Appl. Phys. A*, 2008, **90**, 637-643.
15. A. V. Naumov, S. Ghosh, D. A. Tsyboulski, S. M. Bachilo and R. B. Weisman, *ACS Nano*, 2011, **5**, 1639-1648.
16. J. Fagan, N. Lin, R. Zeisler and A. Hight Walker, *Nano Res.*, 2011, **4**, 393-404.
17. Y. Tian, H. Jiang, J. v. Pfaler, Z. Zhu, A. G. Nasibulin, T. Nikitin, B. Aitchison, L. Khriachtchev, D. P. Brown and E. I. Kauppinen, *The Journal of Physical Chemistry Letters*, 2010, **1**, 1143-1148.
18. Y. Murakami, E. Einarsson, T. Edamura and S. Maruyama, *Physical Review Letters*, 2005, **94**, 087402.
19. Y. R. Park, W.-J. Kim, M. J. Ko, N. K. Min and C. J. Lee, *Nanoscale*, 2012, **4**, 6532-6536.
20. Y. Murakami and S. Maruyama, *Physical Review B*, 2009, **79**, 155445.
21. E. A. Taft and H. R. Philipp, *Physical Review*, 1965, **138**, A197-A202.
22. V. G. Kravets, A. N. Grigorenko, R. R. Nair, P. Blake, S. Anissimova, K. S. Novoselov and A. K. Geim, *Physical Review B*, 2010, **81**, 155413.
23. L. Yang, J. Deslippe, C.-H. Park, M. L. Cohen and S. G. Louie, *Physical Review Letters*, 2009, **103**, 186802.
24. K. F. Mak, J. Shan and T. F. Heinz, *Physical Review Letters*, 2011, **106**, 046401.
25. J. J. Crochet, S. Hoseinkhani, L. Lüer, T. Hertel, S. K. Doorn and G. Lanzani, *Physical Review Letters*, 2011, **107**, 257402.
26. R. Kiebooms, R. Menon and K. lee, in *Handbook of Advanced Electronic and Photonic Materials and Devices*, ed. H. S. Nalwa, Academic Press, Burlington2001, pp. 64-65.
27. K. Liu, J. Deslippe, F. Xiao, R. B. Capaz, X. Hong, S. Aloni, A. Zettl, W. Wang, X. Bai, S. G. Louie, E. Wang and F. Wang, *Nat Nano*, 2012, **7**, 325-329.
28. X. Tu, A. Walker, C. Khripin and M. Zheng, *Journal of Ameciran Chemical Society*, 2011, **133**, 12998-13001.
29. F. Vialla, C. Roquelet, B. Langlois, G. Delport, S. M. Santos, E. Deleporte, P. Roussignol, C. Delalande, C. Voisin and J.-S. Lauret, *Physical Review Letters*, 2013, **111**, 137402.
30. M. F. Islam, D. E. Milkie, C. L. Kane, A. G. Yodh and J. M. Kikkawa, *Physical Review Letters*, 2004, **93**, 037404.
31. K. Liu, X. Hong, S. Choi, C. Jin, R. B. Capaz, J. Kim, W. Wang, X. Bai, S. G. Louie, E. Wang and F. Wang, *Proceedings of the National Academy of Sciences*, 2014, **111**, 7564-7569.
32. H. Jiang, J. Ruokolainen, N. Young, T. Oikawa, A. G. Nasibulin, A. Kirkland and E. I. Kauppinen, *Micron*, 2012, **43**, 545-550.
33. H. Jiang, A. G. Nasibulin, D. P. Brown and E. I. Kauppinen, *Carbon*, 2007, **45**, 662-667.
34. H. Jiang, D. P. Brown, P. Nikolaev, A. G. Nasibulin and E. I. Kauppinen, *Applied Physics Letters*, 2008, **93**, 141903.
35. A. V. Krasheninnikov and F. Banhart, *Nat Mater*, 2007, **6**, 723-733.

RSC Advances Accepted Manuscript